Wavelet-Based Fluid Motion Estimation

Pierre Dérian, Patrick Héas, Cédric Herzet, and Étienne Mémin

INRIA Rennes-Bretagne Atlantique,
Campus universitaire de Beaulieu, 35042 Rennes Cedex, France.
{Pierre.Derian,Patrick.Heas,Cedric.Herzet,Etienne.Memin}@inria.fr
http://irisa.fr/fluminance

Abstract. Based on a wavelet expansion of the velocity field, we present a novel optical flow algorithm dedicated to the estimation of continuous motion fields such as fluid flows. This scale-space representation, associated to a simple gradient-based optimization algorithm, naturally sets up a well-defined multi-resolution analysis framework for the optical flow estimation problem, thus avoiding the common drawbacks of standard multi-resolution schemes. Moreover, wavelet properties enable the design of simple yet efficient high-order regularizers or polynomial approximations associated to a low computational complexity. Accuracy of proposed methods is assessed on challenging sequences of turbulent fluids flows.

Keywords: Optical flow, continuous fluid motion, wavelet multi-resolution analysis, high-order regularization, polynomial approximation.

1   Introduction

Recent years have seen significant progress in signal processing techniques for fluid motion estimation. The wider availability of image-like data, whether coming from experimental facilities (e.g. particle image velocimetry) or from larger-scale geophysical study systems such as lidars or meteorological and oceanographical satellites, strongly motivates the development of computer-vision methods dedicated to their analysis. Correlation-based and variational methods have proven to be efficient in this context. However, the specific nature of fluid motion highly complicates the process. Indeed, one has to deal with continuous fields showing complex structures evolving at high velocities. This is particularly problematic with optical flow methods, where the problem non-linearity requires to resort to an ad-hoc multi-resolution strategy. Although leading to good empirical results, this technique is known to have a number of drawbacks. Moreover, the underdetermined nature of the optical flow estimation problem imposes to add some prior information about the sought motion field. In many contributions dealing with rigid-motion estimation, first-order regularization is considered with success. However, when tackling more challenging problems such as motion estimation of turbulent fluids, this simple prior turns out to be inadequate. Second-order regularizers allowing to enforce physically-sound properties

of the flow are considered [2, 4, 10, 11], but their implementation raises up several issues.

In this paper, we propose an optical-flow estimation procedure based on a wavelet expansion of the velocity field. This approach turns out to offer a nice mathematical framework for multi-resolution estimation algorithms, which avoids some of the drawbacks of the usual approach. Note that algorithms based on wavelet expansion of the data [1] or the velocity field [9] have been previously proposed. However, unlike the algorithm presented hereafter, the computational complexity of the later seriously limits its application to small images and/or the estimation of the coarsest motion scales. Moreover, we consider the effective implementation of high-order regularization schemes, based upon very simple constraints on the wavelet coefficients at small scales. We finally assess the relevance of proposed methods on challenging image sequences of turbulent fluid motions. Simulation results prove that the proposed approach outperforms the most effective state-of-the-art algorithms.

2   Optical Flow Background

Optical flow estimation is an ill-posed inverse problem. It consists in estimating the apparent motion of a 3D scene through image brightness $I(\boldsymbol{x}, t)$ variations in space $\boldsymbol{x} = (x_1, x_2)^T \in \Omega \subset \mathbb{R}^2$ and time $t \in \mathbb{R}$. Optical flow, identified by a 2D velocity field $\boldsymbol{v}(\boldsymbol{x}, t) : \Omega \times \mathbb{R}^+ \mapsto \mathbb{R}^2$ is the projection on the image plane of the 3D scene velocity. Its estimation involves two main aspects: a *data model* that links image data to the velocity field and a *regularization* scheme to overcome the ill-posedness.

2.1   Non-Linear Data Model

Data models are commonly built upon assumptions about the temporal variations of the image brightness. The integration of a conservation assumption leads to the well-known *Displaced Frame Difference* (DFD) equation, which is studied in the following. However, the approach remains valid for any other integrated data model. Let us denote by $I_0(\boldsymbol{x})$ and $I_1(\boldsymbol{x})$ two consecutive image samples of the continuous sequence $I(\boldsymbol{x}, t)$ which has been discretized in time with a unit interval. Under rigid motion and stable lighting conditions, $\boldsymbol{v} = (v_1, v_2)^T$ satisfies the standard DFD equation, which reads:

$$\forall \boldsymbol{x} \in \Omega, \ f_{\mathrm{DFD}}(I, \boldsymbol{v}) = I_1(\boldsymbol{x} + \boldsymbol{v}(\boldsymbol{x})) - I_0(\boldsymbol{x}) = 0 \ . \tag{1}$$

The estimated motion field $\hat{\boldsymbol{v}}$ is obtained by minimizing a cost function, which we chose quadratic in the following to clarify the presentation:

$$\hat{\boldsymbol{v}} = \arg\min_{\boldsymbol{v}} J_{\mathrm{DFD}}(I, \boldsymbol{v}) \ , \ \text{with} \ J_{\mathrm{DFD}}(I, \boldsymbol{v}) = \frac{1}{2} \int_{\Omega} |f_{\mathrm{DFD}}(I, \boldsymbol{v})|^2 d\boldsymbol{x} \ . \tag{2}$$

The data model being non-linear w.r.t. the velocity field $\boldsymbol{v}$, estimation of optical flow therefore requires a specific optimization approach.

2.2 Classical Multi-resolution Strategy

Indeed, the equations for the inversion are only valid if the solution remains in the linearity region of the image intensity function. A standard approach for tackling non-linearity is to rely on an incremental multi-resolution strategy. This approach consists in choosing some sufficiently coarse low-pass-filtered version of the images at which the linearity assumption is valid, and to estimate a first displacement field assumed to correspond to a coarse representation of the motion. Then, a so-called Gauss-Newton strategy is used by applying successive linearizations around the current estimate and warping accordingly a representation of the images of increasing resolution. More explicitly, let us introduce the following incremental decomposition of the displacement field at resolution[1] 2^j:

$$\boldsymbol{v}_j = \tilde{\boldsymbol{v}}_j + \boldsymbol{v}'_j \tag{3}$$

where $\boldsymbol{v}'_j$ represents the unknown incremental displacement field at resolution 2^j and $\tilde{\boldsymbol{v}}_j \triangleq \sum_{i<j} \mathcal{P}_j(\boldsymbol{v}'_i)$ is a coarse motion estimate computed at the previous scales; $\mathcal{P}_j(\boldsymbol{v}'_i)$ denotes a projection operator which projects $\boldsymbol{v}'_i$ onto the grid considered at resolution 2^j. In order to respect the Shannon sampling theorem, the coarse scale data term is derived by a low-pass filtering of the original images with a kernel[2] $\mathcal{G}_j$, followed by a subsampling at period 2^j. Using (3), at coarse scale, image $I_j(\boldsymbol{x})$ and the *motion-compensated* image $\tilde{I}_j(\boldsymbol{x})$ are then defined as:

$$\begin{cases} I_j(\boldsymbol{x}) = \downarrow_{2^j} \circ (\mathcal{G}_j \star I_0(\boldsymbol{x})) \\ \tilde{I}_j(\boldsymbol{x}) = \downarrow_{2^j} \circ (\mathcal{G}_j \star I_1(\boldsymbol{x} + \tilde{\boldsymbol{v}}_j(\boldsymbol{x}))) , \end{cases} \tag{4}$$

where $\downarrow_{2^j}$ denotes a 2^j-periodic subsampling operator. It yields a functional J^j_{OBS} defined as a linearized version of (1) around $\tilde{\boldsymbol{v}}_j(\boldsymbol{x})$:

$$J^j_{\text{OBS}}(I_j, \boldsymbol{v}'_j) = \frac{1}{2} \int_{\Omega_j} \left[\tilde{I}_j(\boldsymbol{x}) - I_j(\boldsymbol{x}) + \boldsymbol{v}'_j(\boldsymbol{x}) \cdot \nabla \tilde{I}_j(\boldsymbol{x}) \right]^2 d\boldsymbol{x} . \tag{5}$$

Finally, the sought motion estimate $\hat{\boldsymbol{v}}$ is given by solving a system of coupled equations associated to resolutions increasing from 2^C to 2^F:

$$\begin{cases} \hat{\boldsymbol{v}} = \boldsymbol{v}'_F + \tilde{\boldsymbol{v}}_F = \boldsymbol{v}'_F + \sum_{i=C}^{F-1} \mathcal{P}_F(\boldsymbol{v}'_i) , \\ \boldsymbol{v}'_j = \arg\min_{\boldsymbol{v}'} J^j_{\text{OBS}}(I_j, \boldsymbol{v}') , \forall j \in \{C, \cdots, F\} . \end{cases} \tag{6}$$

where the finest scale $s = 2^{-F}$ corresponds to the pixel whereas the coarsest scale is noted $s = 2^{-C}$. In practice, equations in (6) are usually solved independently, starting from the coarsest to the finest scale. This coarse-to-fine approach has the

---

[1] In this paper, we shall use the following convention: indices $j \geq 0$ represent the *resolution* 2^j —contrary to [7]. Corresponding *scale* is 2^{-j}.

[2] A Gaussian kernel of variance proportional to 2^j is commonly used.

drawback of freezing (i.e. leaving unchanged), at a given scale, all the previous coarser estimates. Moreover, the major weakness of this strategy is the arbitrary approximation of the original functional in (2) by a set of coarse scale data terms (5), which are defined at different resolutions by a modification of original input images with (4) and by a linearization of model (1) around the previous motion estimate. In the next section, we will see that this multi-resolution strategy has a mathematically-sound formulation within the framework of wavelet representations.

2.3   The Aperture Problem and Usual Regularization Schemes

Previously introduced data models remain under-constrained, as they provide for each time t a single equation for two unknowns (v_1, v_2) at each spatial location $\boldsymbol{x} = (x_1, x_2)^T$. To deal with this under-constrained estimation problem, the most common setting consists in enforcing some spatial coherence to the solution.

Implicit Regularization The motion field is constrained to be of the form $\boldsymbol{v} = \Phi(\Theta)$, where Φ is a function parametrized by Θ (piece-wise polynomial functions are often used). Implicit regularization schemes penalize discrepancies from model (1) by minimizing J_{DFD} with respect to Θ, i.e.

$$\hat{\boldsymbol{v}} = \Phi\Big(\arg\min_{\Theta} J_{\mathrm{DFD}}(I, \Phi(\Theta)) \Big) \; . \tag{7}$$

Associated to a low-order parametric representation, this simple approach reduces drastically the dimension of the problem, hence addressing its under-constrained nature. However, when spatiotemporal gradients of the images vanish, it is impossible to guarantee the existence of an unique solution: this is the *aperture problem*.

Explicit Regularization Global regularization schemes in their simplest form define the estimation problem through the minimization of a functional composed of two terms balanced by a regularization coefficient $\mu > 0$:

$$J(I, \boldsymbol{v}, \mu) = J_{\mathrm{DFD}}(I, \boldsymbol{v}) + \mu J_{\mathrm{reg}}(\boldsymbol{v}) \; . \tag{8}$$

Thus, motion estimate $\hat{\boldsymbol{v}}$ satisfies $\hat{\boldsymbol{v}} = \arg\min_{\boldsymbol{v}} J(\boldsymbol{v}, I, \mu)$. The data term J_{DFD} is still defined by (2) . The second term, J_{reg} (the "regularization term"), encourages the solution to follow some prior smoothness model formalized with function f_{reg}:

$$J_{\mathrm{reg}}(\boldsymbol{v}) = \frac{1}{2} \int_{\Omega} f_{\mathrm{reg}}(\boldsymbol{v}, \boldsymbol{x}) d\boldsymbol{x} \; . \tag{9}$$

An n-order regularization writes in its simplest form:

$$f_{\mathrm{reg}}(\boldsymbol{v}, \boldsymbol{x}) = \sum_{i=1,2} \sum_{j=1,2} \left| \frac{\partial^n v_i}{\partial x_j^n}(\boldsymbol{x}) \right|^2 \; . \tag{10}$$

A first-order regularizer (i.e. $n = 1$) enforcing weak spatial gradients of the two components v_1 and v_2 of the velocity field $\boldsymbol{v}$ is very often used [6]. Second-order regularizers (i.e. $n > 1$) have been proposed in the literature in the case of fluid flows [2, 10, 11]. However, since motion variables are considered on the pixel grid, an approximation of continuous spatial derivatives by discrete operators is required. For regular pixel grids, it is usually done using finite difference schemes. Nevertheless, it is well known that ensuring stability of the discretization schemes of high-order regularizer may constitute a difficult problem.

3 Wavelet Formulation

As shown in Sect. 2, the common optical flow estimation approach suffers from two main drawbacks: the necessary "empirical" multi-resolution approach and the implementation of efficient regularizations terms. The use of wavelet bases is a simple answer to both problems. Moreover, it has been shown that a wavelet expansion is appropriate for representing turbulent flows [3].

3.1 Wavelet Decomposition

In order to avoid the limitations of the classical multi-resolution strategy, we consider the projection of each scalar component v_1, v_2 of the velocity field $\boldsymbol{v}$ onto *multi-resolution approximation spaces* exhibited by the wavelet formalism. Let us introduce briefly this context for real 1D scalar signals. We consider a multi-resolution approximation of $\mathbf{L}^2(\mathbb{R})$ as a sequence $\{V_j\}_{j \in \mathbb{Z}}$ of closed subspaces, so-called *approximation spaces*, notably verifying[3]

$$V_j \subset V_{j+1} \; ; \lim_{j \to -\infty} V_j = \bigcap_{j=-\infty}^{+\infty} V_j = \{0\} \; ; \lim_{j \to +\infty} V_j = \text{Closure} \left(\bigcup_{j=-\infty}^{+\infty} V_j \right) = \mathbf{L}^2(\mathbb{R}) \; .$$

Since approximation spaces are sequentially included within each other, they can be decomposed: $V_{j+1} = V_j \oplus W_j$. Those W_j are the orthogonal complements of approximation spaces, they are called *detail spaces*.

Practically, scalar 1D signals being finite, they belong to a given approximation space according to their resolution, i.e. number of samples. Let w be a 1D signal of 2^{F+1} samples, then $w \in V_{F+1} = V_C \oplus W_C \oplus W_{C+1} \oplus \cdots \oplus W_F \subset \mathbf{L}^2([0, 1])$, where $0 \leq C \leq F$. The projection of w on this multiscale basis writes:

$$w(x) = \sum_{k=0}^{2^C - 1} \langle w, \phi_{C,k} \rangle_{\mathbf{L}^2} \phi_{C,k}(x) + \sum_{j=C}^{F} \sum_{k=0}^{2^j - 1} \langle w, \psi_{j,k} \rangle_{\mathbf{L}^2} \psi_{j,k}(k) \; . \qquad (11)$$

Here, $\{\phi_{C,k}\}_k$ and $\{\psi_{j,k}\}_k$ are orthonormal bases of V_C and W_j, respectively. They are defined by *dilatations* and *translations*[4] of the so-called *scale function*

---

[3] See [7] for a complete presentation of wavelet bases.
[4] Written in a general form $f_{j,k}(x) = 2^{j/2} f(2^j x - k)$.

ϕ and its associated *wavelet function* ψ. Functions ϕ and ψ verify the following two-scale relations:

$$\phi(x) = \sqrt{2}\sum_{k\in\mathbb{Z}} h[k]\phi(2x-k) \,;\; \psi(x) = \sqrt{2}\sum_{k\in\mathbb{Z}} g[k]\phi(2x-k)\,, \qquad (12)$$

where sequences $h[k] = \langle \phi(x), \sqrt{2}\phi(2x-k)\rangle$ and $g[k] = \langle \psi(x), \sqrt{2}\phi(2x-k)\rangle$ are called *conjugate mirror filters*. Those filters play an important role in the fast implementation with *filter banks* of forward and inverse wavelet transform, i.e. projection on the wavelet basis and reconstruction, from (11) [7]. Finally, the representation of a signal projected onto the multiscale wavelet basis is given by the set of coefficients appearing in (11): $a_{C,k} \triangleq \langle w, \phi_{C,k}\rangle_{\mathbf{L}^2}$ and $d_{j,k} \triangleq \langle w, \psi_{j,k}\rangle_{\mathbf{L}^2}$ are approximation and detail coefficients, respectively. Those results are extended to the case of 2D signals, in order to obtain *separable multiscale orthonormal bases* of $\mathbf{L}^2([0,1]^2)$.

3.2   Wavelet Data Term

In this work, the representation of the velocity field $\boldsymbol{v}$ is obtained by the wavelet decomposition (11) of each component. We denote by Θ_1 and Θ_2 the sets of coefficients respectively associated to v_1 and v_2; $\Theta = (\Theta_1, \Theta_2)^T$ is the set of all coefficients. Denoting the linear reconstruction operator by Φ for convenience, we may write

$$\forall \boldsymbol{x} \in \Omega, \; \boldsymbol{v}(\boldsymbol{x}) = \Phi(\boldsymbol{x})\Theta\,. \qquad (13)$$

Here the constant coefficients vector Θ is the unknown of our optical flow estimation problem. Replacing $\boldsymbol{v}(\boldsymbol{x})$ by (13) in DFD data term (1), we obtain

$$J_{\mathrm{DFD}}(\Theta) = \frac{1}{2}\int_{\Omega}\left[I_1(\boldsymbol{x}+\Phi(\boldsymbol{x})\Theta) - I_0(\boldsymbol{x})\right]^2 d\boldsymbol{x} \qquad (14)$$

and the estimation problem becomes

$$\hat{\boldsymbol{v}} = \Phi\hat{\Theta} \in V_{F+1}\,, \;\text{ where } \hat{\Theta} = \arg\min_{\Theta} J_{\mathrm{DFD}}(\Theta)\,. \qquad (15)$$

3.3   Multiscale Estimation

Unknown coefficients are estimated sequentially from coarsest scale C to a chosen finest one L (with $C \le L \le F$) using a gradient-descent algorithm. At each scale j, all coefficients from scales C to j are estimated. Coefficients previously estimated at coarser approximation spaces are used to initialize the gradient descent; this strategy enables the update of the latter coarser coefficients while estimating "new" details at current scale j. In other words, solution $\hat{\boldsymbol{v}}$ is sequentially sought within higher resolution spaces: $V_C \subset V_{C+1} \subset \cdots \subset V_L$. This way, the projection of the current solution $\hat{\boldsymbol{v}} \in V_j$ onto every coarser space V_p with $C \le p < j$ is constantly updated, contrary to the standard incremental approach (Sect. 2.2). The use of wavelet bases thus leads to a "natural" and well-defined multi-resolution framework. At each refinement level, minimization of functional

J_{DFD} is efficiently achieved with a gradient-based quasi-Newton algorithm (L-BFGS) [8], to seek the optimum $\hat{\Theta}$. For any coefficient $\theta_{i,p} \in \Theta_i \subset \Theta$,

$$\frac{\partial J_{\text{DFD}}}{\partial \theta_{i,p}}(\Theta) = \left\langle \frac{\partial I_1}{\partial x_i}(\cdot + \Phi(\cdot)\Theta)\left[I_1(\cdot + \Phi(\cdot)\Theta) - I_0(\cdot)\right], \Phi_p \right\rangle_{\mathbf{L}^2([0,1]^2)} \tag{16}$$

where Φ_p is the wavelet basis atom related to $\theta_{i,p}$. As a consequence, components of the spatial gradient of the data-term functional (14) are simply given by the coefficients of the wavelet decomposition of the two terms

$$\frac{\partial I_1}{\partial x_i}(\boldsymbol{x} + \Phi(\boldsymbol{x})\Theta)\left[I_1(\boldsymbol{x} + \Phi(\boldsymbol{x})\Theta) - I_0(\boldsymbol{x})\right], \quad i = 1, 2,$$

on the considered wavelet basis. It is easy to see that the proposed coarse-to-fine estimation strategy enables to capture large displacements: at large scales, the decomposition of (3.3) is obtained by convolutions with the atoms of the wavelet basis having the largest support. Note that conversely to the algorithm proposed in [9], the low-complexity of gradient computation via fast wavelet transform does not restrict motion estimation to large scales and/or images of small size.

4 Regularizations

4.1 Wavelet Properties

Wavelet-based regularizers which are described in the following are based upon wavelet properties such as polynomial reproduction, differentiation and interpolation. Those aspects are linked to the notion of *vanishing moments* (VM). A wavelet $\psi(x) \in \mathbf{L}^2(\mathbb{R})$ has n VM if :

$$\int_{\mathbb{R}} x^\ell \psi(x) dx = 0, \text{ for } 0 \leq \ell < n . \tag{17}$$

Wavelets as polynomial approximations From (17), a wavelet with n VM is hence orthogonal to any polynomial of degree $n-1$. Consequently, piece-wise[5] polynomials of degree $n - 1$ belonging to V_{F+1} are exactly described in V_F, since the atoms of the basis that belong to its orthogonal complement W_F have vanishing coefficients.

Wavelets as Differential Operators Given a signal $w \in \mathcal{C}^n$, the behavior of its small scales coefficients resulting from an n-VM wavelet decomposition can be related to its nth derivative [7]:

$$\lim_{j \to \infty} \frac{\langle w(x), \psi_{j,k}(x) \rangle}{2^{-j(n+\frac{1}{2})}} \propto \frac{\partial^n w(x)}{\partial x^n} . \tag{18}$$

This result can be extended to the case of 2D signals.

---

[5] On the support of $\{\psi_{F,k}\}$.

Wavelet-Based Interpolation A multiscale interpolation is the orthogonal projection of a signal w estimated at a given resolution 2^j onto the next finer approximation space V_{j+1}:

$$P_{V_{j+1}} w \left(2(p + \frac{1}{2}) \right) = \sum_{k=-\infty}^{+\infty} w(2k) \varphi_{j+1}(p - k + 1/2) . \qquad (19)$$

The interpolation function φ is defined as the autocorrelation of the scaling function: $\varphi = \phi \star \breve{\phi}$, where $\star$ and $\breve{}$ denote respectively convolution and time-reverse[6] operators. It can be shown that φ interpolates exactly polynomials of order n if and only if the wavelet associated to scaling function ϕ has $n + 1$ VM [7]. This linear interpolation operator $P_{V_{j+1}}$ is also implemented with filter banks using filter h_i, where $h_i[n] = \left(h \star \breve{h} \right) [2n + 1]$ and h is defined in (12).

4.2   Polynomial Approximation on a Truncated Basis

As seen in Sect. 2.3, a first way to overcome the under-constrained nature of the optical flow estimation problem consists in reducing the number of unknowns through a parametric formulation of the velocity field. Using the proposed wavelet formulation (15), this can be easily achieved by estimating the velocity field on a truncated wavelet basis. This means that the solution $\hat{\boldsymbol{v}}$ belongs to a lower-resolution space $V_L \subset V_{F+1}$ and therefore is a piece-wise polynomial of order $n - 1$ in V_{L+1}. Details coefficients associated to non-estimated small details scales (W_j with $L \leq j \leq F$) are thus not estimated, but set to zero.

$$\hat{\boldsymbol{v}} = \Phi \hat{\Theta} \in V_L \, , \; L < F + 1 \, , \; \text{where } \hat{\Theta} = \arg \min_{\Theta} J_{\text{DFD}}(\Theta) \, . \qquad (20)$$

Since the basis truncation reduces the number of unknowns, it is theoretically possible to estimate detail coefficients up to penultimate scale $F - 1$, i.e. $\hat{\boldsymbol{v}} \in V_F$. Practically, it is impossible due to the aperture problem.

4.3   High-Order Regularization

It has been previously mentioned that smallest scale coefficients might be interpreted as the signal's n^{th} derivative (Sect. 4.1), with n number of VM of the considered wavelet. The penalization of small scale coefficients' amplitude thus enables to control the amplitude of the derivative of the estimated signal. However, due to the dyadic structure of the discrete wavelet decomposition, only a "piecewise" control is possible. In order to control the derivative at junctions of those dyadic blocks, *interpolated signal* $\tilde{\boldsymbol{v}}$ of the velocity field $\boldsymbol{v}$ on a shifted 2D grid is considered. Small scale coefficients $\{\tilde{\Theta}_F\}$ and $\{\Theta_F\}$ of both $\tilde{\boldsymbol{v}}$ and $\boldsymbol{v}$ are penalized. "Interpolated coefficients" $\tilde{\Theta}$ are expressed as a linear combination of Θ through wavelet inverse and forward transformations (Φ, $\Phi^{-1} = \Phi^T$, resp.)

---

[6] More explicitly, $\breve{f} : \; t \mapsto \breve{f}(t) = f(-t)$.

and interpolation: $\tilde{\Theta} = \left(\Phi^T \circ P_{V_{F+1}} \circ \Phi\right)\Theta$. We finally get the regularization term

$$J_{\text{reg}}(\Theta) = \frac{1}{2}\|\Theta_F\|^2 + \frac{1}{2}\|\tilde{\Theta}_F\|^2 \text{ and } \nabla J_{\text{reg}}(\Theta) = \Theta_F + \left(\Phi^T \circ P_{V_{F+1}}^T \circ \Phi\right)\tilde{\Theta}_F \quad (21)$$

The gradient in (21) is a linear form which can be efficiently computed using the recursive filter banks presented in Sect. 3.1 and 4.1. The addition of the regularization term (21) therefore does not increase significantly the computational burden. Supplementing (15), the estimation problem becomes:

$$\hat{\boldsymbol{v}} = \Phi\hat{\Theta} \in V_{F+1}, \text{ where } \hat{\Theta} = \arg\min_{\Theta} J_{\text{DFD}}(\Theta) + \mu J_{\text{reg}}(\Theta). \quad (22)$$

5   Results

Daubechies wavelets have been chosen since they have a minimum support size for a given number of VM [7]. Daubechies wavelet with n VM will be referred to as D_n hereafter. Wavelet transform is implemented with periodic boundary conditions.

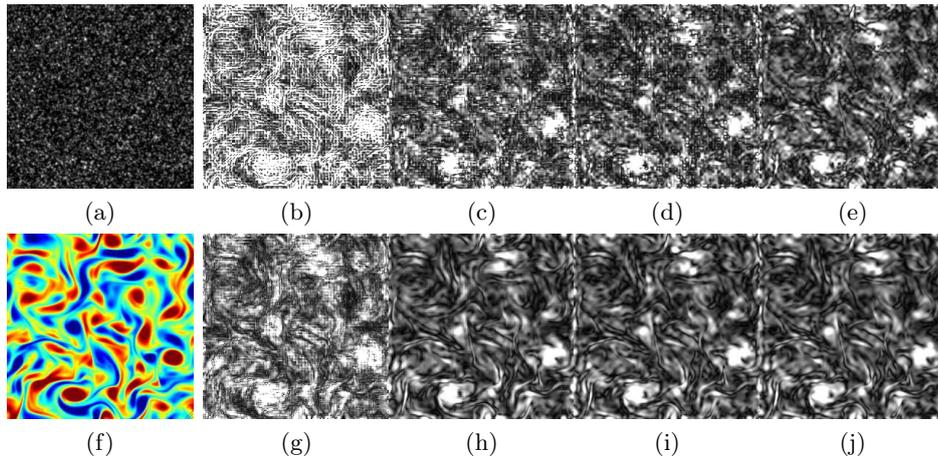### 5.1   Synthetic PIV Sequence

Fig. 1. Sample synthetic *PIV image* (1a) with below the *vorticity* of the underlying reference velocity field (1f). End-point error maps on velocity field estimations for a polynomial approximation (*upper row*) and high-order regularization (*lower row*) with D_n wavelets are presented, i.e. polynomial (resp. derivative) order of $n-1$ (resp. n), for D_1 (1b, 1g), D_2 (1c, 1h), D_3 (1d, 1i) and D_{10} (1e, 1j).

The first data set used for evaluation is a synthetic sequence of Particle Imagery Velocimetry (PIV) images of size 256×256 pixels, representing small particles (of radius below 4 pixels) advected by a 2D periodic forced turbulent

flow. The dynamic of the fluid flow is given by numerical simulation of 2D Navier-Stokes equations at $Re = 3000$, using the vorticity conservation equation and the Lagrangian equation for non-heavy particles transported by the flow (simulation details can be found in [5]). This simulated flow has a null-divergence by construction. An image of the PIV sequence is displayed in Fig. 1a together with its associated ground truth motion vorticity (1f). Estimated velocity field evaluation is based on the Root Mean Square end-point Error (RMSE)[7].

When the true velocity field is decomposed on a Daubechies wavelet with a number of VM higher than 3, the velocity field reconstructed with the $p = 6$ coarser scales (out of 8) carries out more than 99,95% of the total kinetic energy. Those 6 scales are represented with only 12.5% of atoms from the full wavelet basis. Moreover, when n is chosen high enough (> 7), the reconstruction error stabilizes around $0, 013$.

Motion Estimation From the previous analysis of the true velocity fields, it seems that 6 detail scales out of 8 should give an accurate representation of the motion in terms of kinetic energy, as long as the chosen number of VM is high enough. Figure 2a (black curve) shows RMS errors computed on an estimated velocity field with truncated Daubechies wavelet bases (Sect. 4.2) having different VM n, i.e. with a polynomial approximation of order $n - 1$. As expected, RMSE converges rapidly towards a median value of 0.0613 when n increases. Figure 1 (upper row) shows corresponding end-point error maps for motion estimated with wavelets bases D_1, D_2, D_3 and D_{10}. Although errors effectively lower when higher VM wavelets are employed, artifacts due to high-amplitude errors on 6th scale coefficients (small white "dots") and on coarse coefficients (white straight "lines") remain clearly visible. With the proposed high-order regularization scheme (Sect. 4.3), all scales are estimated, which should highly improve results with $n \leq 3$ VM, i.e. for penalization of derivatives of order lower than 3. This is confirmed on Fig. 2a (red dashed curve), with a reduction of 35% and 30% of the RMS obtained with D_1 and D_2 wavelets bases, respectively, whereas the diminution observed using D_{10} wavelet basis is of 10% at best. At the same time, derivative penalization eliminates most of the artifacts observed on estimates with truncated bases, which is displayed on the lower row of Fig. 1. Note also that there are less differences between estimations with different VM, in comparison to the previous case.

Comparison with State-of-the-Art Estimators Figure 2 is a comparison of RMS errors obtained on the synthetic PIV sequence with the proposed high-order regularizer and various state-of-the-art estimators, after a null-divergence projection. Our wavelet-based estimator clearly outperforms other methods.

---

[7] Ground-truth velocity fields being given on a shifted grid (by 1/2 pixel) by the numerical simulation, they have been interpolated in order to compute accurate RMSE on the pixel grid.
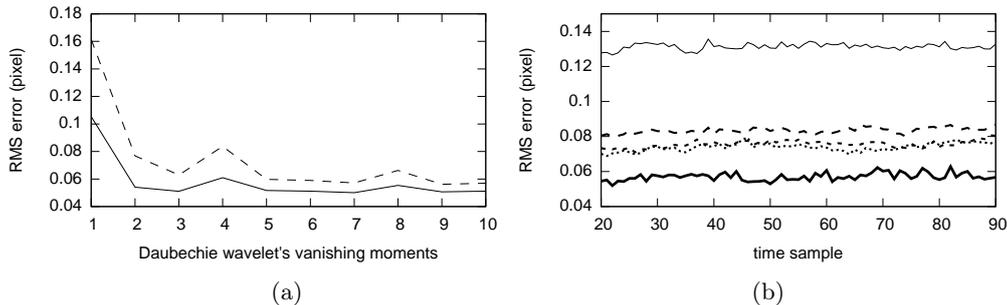
<center>(a)</center>

<center>(b)</center>

Fig. 2. *Left*: Comparison of RMS errors on velocity fields estimated from a pair of the synthetic PIV sequence, with the proposed methods and Daubechies wavelets with 1 to 10 VM, i.e. for polynomial approximation (resp. derivative regularization) of order 0 to 9 (resp. 1 to 10). RMSE obtained with the polynomial approximation (6 scales out of 8, *dashed line*) and with derivatives regularization (best case, *solid line*). *Right*: Comparison of RMS errors on a sequence of velocity fields estimated with proposed regularization (*thick solid*) and with state-of-the-art methods: correlation (*thin solid*), first order regularization [6] (*long-dashed*), div-curl regularization [10] (*dashed*), self-similar regularization [4] (*dotted*).

5.2   Real PIV Sequence

This data set consists in 128 PIV pictures of a transversal view of a planar concomitant jet flow, of size 1024×1024 pixels. The flow has a "top-hat" velocity profile and is poorly turbulent, but shows two high-shear regions featuring development of Kelvin-Helmholtz instabilities. Motion is estimated with proposed wavelet-based estimator (22), using the following settings: 2 VM and derivatives penalization with factor $\mu = 10^7$. Figure 3 presents a PIV image of the sequence and streamlines of an estimated velocity field along with two consecutive vorticity maps. A qualitative evaluation of the presented motion field shows a remarkably good agreement with the physics of concomitant jets. A very good temporal coherence is also observed, although no prior dynamic model is considered (i.e. successive pairs of images are processed independently).

6   Conclusion

An optical flow estimation algorithm dedicated to continuous motion has been introduced. The choice of the wavelet formalism sets-up a well-defined multi-resolution framework that avoids most drawbacks of such usual approaches. Being associated to a gradient-based quasi-Newton optimization method, its low complexity makes possible the estimation of the full range of scales composing the motion. Moreover, high numbers of vanishing moments enable to truncate the wavelet basis without increasing the error of the polynomial reconstruction, thus significantly reducing the number of unknowns and the problem complexity. A high-order regularization scheme, involving small scale coefficients penalization, highly enhances estimation results and generally helps reducing errors by removing noise of the solution, as emphasized by experiments on a synthetic PIV sequence. Application to a real PIV sequence shows the capability of the estimation method to reconstruct accurately vortices of large amplitude.
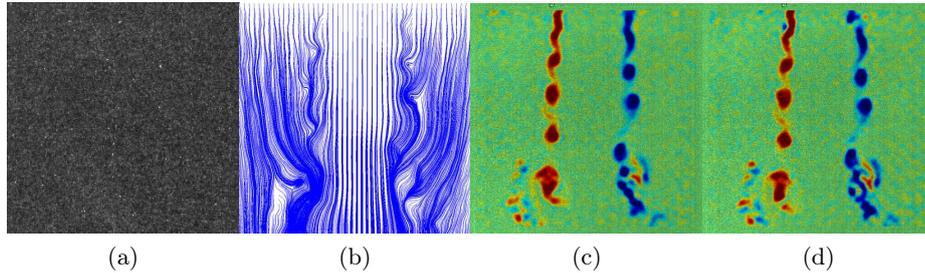
(a)	(b)	(c)	(d)

Fig. 3. Sample estimated motion fields from 2D planar jet PIV dataset: detail of input *PIV image* (3a), *streamlines* (3b) and *vorticity* (3c). Figure 3d is the vorticity field corresponding to motion estimated at the next time step. Three different areas are visible: at the output of the jet (top of the field), shear regions begin to oscillate slowly. The middle region clearly shows the development of vortices characteristic of the Kelvin-Helmholtz instability. Finally, in the lower part of the field, structure of vortices collapse due to their tri-dimensionalization.

Acknowledgments

References

1. Bernard, C.: Wavelets and ill posed problems: optic flow and scattered data interpolation. Ph.D. thesis, École Polytechnique (1999)
2. Corpetti, T., Mémin, E., Pérez, P.: Dense estimation of fluid flows. Pattern Anal Mach Intel 24(3), 365–380 (2002)
3. Farge, M.: Wavelet transforms and their applications to turbulence. Annual Review of Fluid Mechanics 24(1), 395–458 (1992)
4. Heas, P., Memin, E., Heitz, D., Mininni, P.: Bayesian selection of scaling laws for motion modeling in images. In: International Conference on Computer Vision (ICCV'09). Kyoto, Japan (October 2009)
5. Heitz, D., Carlier, J., Arroyo, G.: Final report on the evaluation of the tasks of the workpackage 2, FLUID project deliverable 5.4. Tech. rep., INRIA - Cemagref (2007)
6. Horn, B., Schunck, B.: Determining optical flow. Artificial Intelligence 17, 185–203 (1981)
7. Mallat, S.: A Wavelet Tour of Signal Processing: The Sparse Way. Academic Press (2008)
8. Nocedal, J., Wright, S.J.: Numerical Optimization. Springer Series in Operations Research, Springer-Verlag, New York, NY (1999)
9. Wu, Y., Kanade, T., Li, C., Cohn, J.: Image registration using wavelet-based motion model. Int. J. Computer Vision 38(2), 129–152 (2000)
10. Yuan, J., Schnörr, C., Memin, E.: Discrete orthogonal decomposition and variational fluid flow estimation. Journ. of Math. Imaging & Vison 28, 67–80 (2007)
11. Yuan, J., Schnörr, C., Steidl, G.: Simultaneous higher-order optical flow estimation and decomposition. SIAM Journal on Scientific Computing 29(6), 2283–2304 (2007)